LRP 808/05 October 2005

Time-resolved imaging and spatially-resolved spectroscopy of electrical discharge machining plasma

A. Descoeudres, Ch. Hollenstein, G. Wälder, R. Perez

accepted for publication in
J. of Physics D: Applied Physics

ISSN 0458-5895

Time-resolved imaging and spatially-resolved spectroscopy of electrical discharge machining plasma

A Descoeudres[1], Ch Hollenstein[1], G Wälder[2] and R Perez[2]

[1] Ecole Polytechnique Fédérale de Lausanne (EPFL), Centre de Recherches en Physique des Plasmas, CH-1015 Lausanne, Switzerland

[2] Charmilles Technologies SA, 8-10 rue du Pré-de-la-Fontaine, CH-1217 Meyrin, Switzerland

E-mail: antoine.descoeudres@epfl.ch

Abstract. The plasma created during electrical discharge machining is investigated with imaging and spatially-resolved optical emission spectroscopy. Analysis of the pre-breakdown duration shows that the breakdown is of stochastic nature. Due to presence of gas bubbles created by electrolysis, the breakdown mechanism in water could be different from the one in oil. After the breakdown, the plasma develops very fast (< 50 ns) and then remains stable. The plasma excites a broad volume around the electrode gap, between 50 and 400 μm in diameter depending on the discharge current. The H_α line is emitted from the whole plasma, since the hydrogen atoms originate from the dielectric. On the other hand, spatially-resolved spectroscopy shows that plasma contamination from the electrodes is concentrated in their vicinity. After the discharge, light is still emitted by incandescent metallic particles coming from erosion of the workpiece. Profiles between the electrodes of electron density and of electron temperature have been estimated from spatially-resolved emission spectra. The density is found to slightly increase towards the plasma center, whereas the temperature is quite constant across the plasma (~ 0.7 eV).

1. INTRODUCTION

Electrical Discharge Machining (EDM) is a widely-used machining technique since many years. With this technology, numerous industries produce moulds, dies and finished parts with complex shapes. Compared to other conventional machining techniques, EDM has several advantages: machining of all conductive materials regardless of their hardness, no contact and stress to the workpiece during machining, complex cutting shapes, good finishing surface state and machining precision, for example.

The principle of EDM is to use the eroding effect of electric spark discharges on the electrodes. This effect was first discovered by Priestley in 1770, and has been used in a controlled way for machining since the 1940's [1, 2, 3, 4]. The process consists in successively removing small volumes of workpiece material, molten or vaporized during a discharge. The sparks are created in a flowing dielectric, generally water or oil.

The liquid dielectric plays a crucial role for the electrodes cooling and for the material removal: it increases the removing force on the molten metal when the plasma collapses, then it solidifies the molten metal into small particles, and finally it flushes them off.
Recent EDM improvements in machining speed, accuracy and roughness have been achieved mostly with improvements in robotics, automatization, process control, dielectric, flushing and generator design [5, 6]. The other main research domains are the machining of non-conductive materials such as ceramics [7, 8], micro-machining [9, 10, 11], characterization and improvement in the machined surface quality [12, 13], and modelling of the EDM process [14, 15, 16]. But so far, few studies have been done on the discharge itself, which lies at the heart of the process. Further improvements, especially for micro-machining, require a better control and understanding of the discharge, and of its interaction with the electrodes.
Only a few theoretical and numerical studies on the EDM plasma exist [17, 18, 19, 20], due to the complex physics involved in this process. Furthermore, experimental characterization is lacking. Due to the small size of the plasma, its short duration and its weak luminous intensity, it is difficult to use classical plasma diagnostics. For example, it is impossible to use intrusive methods, such as electrostatic probes. The poor reproducibility of the discharges is also an issue for experimental measurements. Even with fixed discharge parameters, the plasma strongly depends on the dielectric cleanliness and the electrode surfaces and geometry, which are constantly evolving during the process.
Optical emission spectroscopy is one of the only applicable plasma diagnostics for EDM plasma. With this method, the electron temperature, the electron density and the influence of the discharge parameters on the plasma emitted light have been measured [21, 22]. It has also been shown by time-resolved spectroscopy that the EDM plasma is weakly non-ideal, especially in the very beginning of the discharge [22]. Imaging is another applicable diagnostic to EDM discharges. It has already been used, especially to understand the breakdown mechanism [23]. Recently, the influence of adding particles to the dielectric has been studied with a high speed camera [13, 24]. However, the experimental characterization of the EDM plasma is incomplete. For numerical model validation, for example, it is necessary to have a complete spatial and temporal characterization of the plasma.
In this paper, we present a spatio-temporal characterization of the EDM plasma with imaging and optical emission spectroscopy. First, some results concerning the pre-breakdown are given; they show the stochastic nature of the breakdown. Then, the evolution of the plasma, during the discharge and the afterglow, is investigated by imaging. Finally, we show spatially-resolved spectroscopy results: contamination measurements, profiles of the electron density and of the electron temperature.

2. EXPERIMENTAL SETUP

The experimental setup is schematically drawn in figure 1. We use a standard EDM die-sinking machine, with a copper electrode and a steel workpiece. The electrode configuration is point-to-point in order to localize the discharge as much as possible. The servo-controlled movements of the upper electrode are vertical. Water or mineral oil is used as dielectric. The discharge parameters (voltage, current, on-time, off-time, polarity) are controlled by the EDM pulse generator.

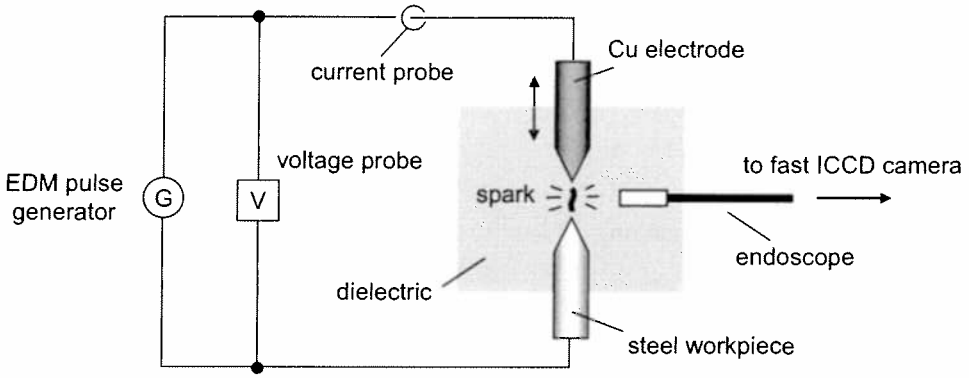

Figure 1. Schematic drawing of the experimental setup for imaging.

The electrical parameters are measured with a differential voltage probe and a 1.6 GHz current transformer probe, connected to a 1 GHz oscilloscope. When breakdown occurs, the current suddenly rises and the gap voltage drops; we use the current rise as a trigger for our diagnostics. Plasma imaging is made with a 30'000 fibres endoscope, directly immersed in the dielectric. The endoscope is equipped with a small lens at its tip, in order to have a magnification of the plasma region. The endoscope has a short working distance: it can be placed a few millimeters from the spark, assuring therefore a good image magnification and small light absorption by the dielectric. The image is detected with a Princeton Instruments PI-MAX camera (intensified CCD camera, < 2 ns gating, 16 bit, 1024×1024 pixels).

Figure 2 shows the experimental setup for spatially-resolved optical emission spectroscopy. In order to have a spatial sampling of the emitted light, the magnified plasma image captured with the endoscope is projected onto an in-line array of 16 fibres. Each fibre collects the light coming from a different zone of the emitting region. The fibres bundle brings the sampled light into a 0.75 m imaging spectrograph ARC SP750i, equipped with three gratings (150, 600 and 1800 g/mm). The 16 different spectra are recorded simultaneously with the same ICCD camera used for imaging. Due to the small size of the light emitting region (see § 3.2.), this arrangement is the easiest way to perform the spatial sampling. In principle, it could be done directly without the endoscope but with an array of fibres directly located near the plasma, but in this case the miniaturization of the fibres in the bundle is then an issue.

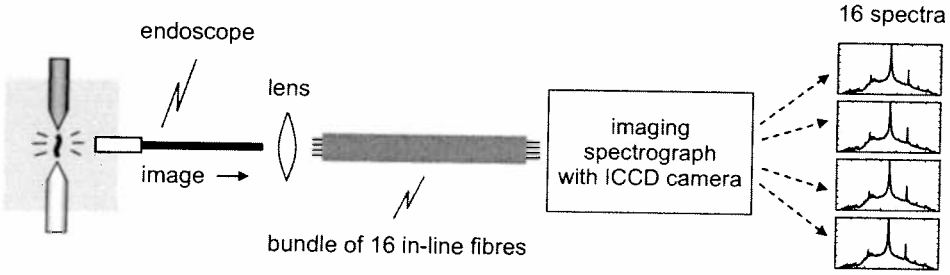

Figure 2. Experimental setup for spatially-resolved spectroscopy. The spatial sampling is obtained by projecting the plasma image onto 16 in-line optical fibres.

3. RESULTS AND DISCUSSION

3.1. Pre-breakdown

When applying a voltage between two electrodes in a dielectric liquid, as in EDM, the electric field has to be sufficiently high to create a breakdown. The breakdown is then not immediate. Studies of pre-breakdown phenomena in dielectric liquids show that different types of streamer exist [25, 26, 27, 28, 29]. A streamer is created at one of the electrodes. This streamer will rapidly grow and propagate towards the other electrode. A streamer carries a certain amount of current because it consists of moving charged species [25]. The streamer structures, velocities and current depend on many parameters such as the gap voltage, the electrode shape and polarity, the gap distance, the chemical and physical properties of the dielectric and its contamination, for example. The breakdown occurs when the streamer reaches the other electrode.

As shown in figure 3, sometimes a fast current signal is measured before the breakdown in water. These current peaks are not associated with the breakdown itself but with the streamer propagation [27, 28, 29]. Each peak represents a streamer which does not completely cross the gap. Each peak can thus be considered as the sign of an uncompleted breakdown.

The measured current peaks reach a few mA and last about 5-20 ns. Assuming a gap of 10-100 μm as generally estimated for EDM discharges, the order of magnitude of the streamer propagation speed is km/s, which is consistent with the literature [26, 27, 28]. We observe this type of current not necessarily just before a breakdown as in figure 3, but randomly as soon as the gap voltage is applied, provided that the electrode spacing is small enough. The water electrical conductivity has an effect on the pre-breakdown current. The number of current peaks per time unit increases with the conductivity. We have not observed any pre-breakdown current in oil in the same condition as in water. However, streamers in oil have been observed in other studies, but with a much higher electric field than the one created with our generator [25, 26, 27, 28].

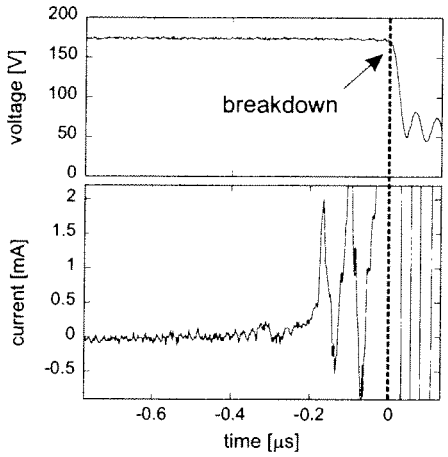

Figure 3. Pre-breakdown current measured in 1.5 μS/cm water (gap voltage 180 V).

In water, many small bubbles can be observed. These bubbles, 30 to 100 μm in diameter, are created by electrolysis of the dielectric. On the other hand, no bubbles are observed during pre-breakdown in oil. Since a streamer is created more easily in a gaseous medium than in a liquid medium, the breakdown mechanism in water could be different from the one in oil, due to presence of gas bubbles.

Once the gap voltage is applied, it takes a certain amount of time until a breakdown occurs. This amount of time is the pre-breakdown duration, also called ignition delay time. The pre-breakdown duration is wasted time from the industrial point of view, because no material removal is performed during it. Statistics of the pre-breakdown duration have been done for discharges with different parameters. The mean pre-breakdown duration differs according to the discharge parameters, but the pre-breakdown duration distribution has always the same shape. Figure 4 shows the histogram of the pre-breakdown duration measured on 8000 similar discharges.

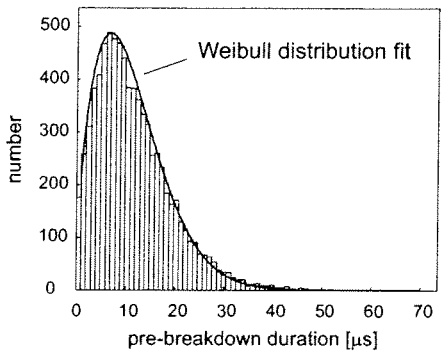

Figure 4. Histogram of the pre-breakdown duration (statistics on 8000 similar discharges: 6 A, 8 μs, -200 V, water).

The distribution of pre-breakdown duration can be well fitted with a Weibull

distribution [30]. This kind of distribution is known for describing, among others, the repartition of the pre-breakdown duration in various dielectric liquids [31, 32]. The breakdown process in EDM has thus a strong stochastic nature. Though we can optimize discharge parameters to reduce the mean pre-breakdown duration, we will always have distributed values. As we will see in the next part, the stochastic nature of the breakdown has a practical consequence for plasma imaging. If it is impossible to predict precisely when the next breakdown will occur, the camera opening for the exposure of a given discharge can only be triggered with the beginning of this very discharge. We cannot anticipate the beginning of the next discharge, as could be done with pulsed RF plasmas, for example.

3.2. Plasma imaging

Figure 5(a) shows a typical image of an EDM plasma. The electrodes have been outlined because they are not visible without an external lighting.

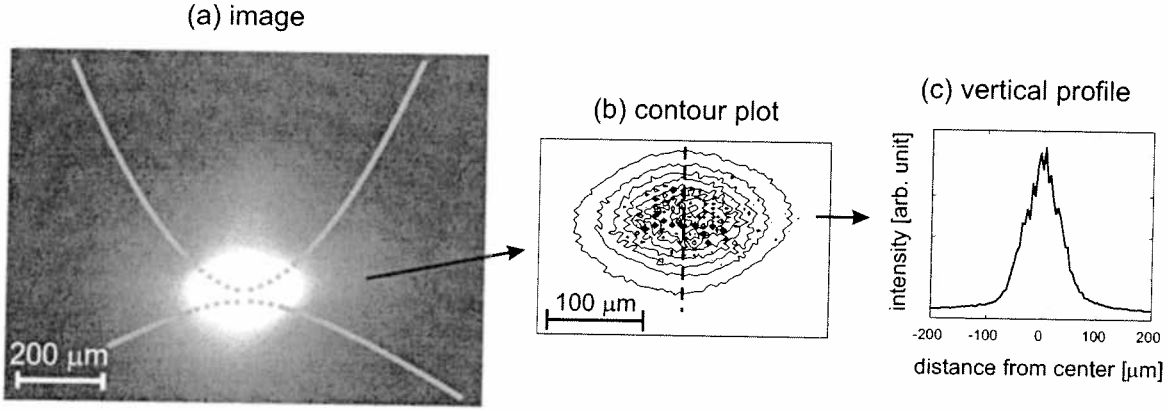

Figure 5. (a) Typical plasma image (5 μs exposure, 5 μs delay after breakdown; 24 A, 100 μs, oil). The position of the electrodes is drawn. (b) Contour plot of (a). (c) Intensity profile of (a) along the vertical axis.

The light emitting region is generally round or oval. Its diameter increases with the discharge current, from 50 to 400 μm for a current increase from 6 to 48 A. But even for the same discharge parameters, plasma images are poorly reproducible. The plasma, and so the shape and size of the emitting region recorded on the images, depend strongly on the electrode surface state, which is constantly evolving during machining. However, the light is mostly originating from a broader region than the gap itself, i.e. the discharge is exciting a broad volume around the electrode gap.

In order to better analyze the images, it is useful to view them as contour and profile plot, as shown in figure 5(b) and 5(c). The dots in the center of figure 5(b), and so the irregularities in the center of figure 5(c), are not real but due to the individual sampling by the endoscope fibres. There are indeed small spaces between the fibres in the endoscope which do not bring the light to the camera. The brightest zone is the

central region (electrode gap) and the light emission decreases rapidly with distance: at 40 μm from the center, the intensity is halved.

The H_α line emitted by neutral hydrogen atoms at 656.2 nm is the dominant contribution in EDM plasma line emission [22]. Imaging of the H_α emission has been measured by adding a band-pass filter centered around 656 nm between the endoscope and the camera. The images obtained are very similar to those obtained without filter. The emitting region has the same shape, size and intensity profiles. Similarly, the intensity evolution of this line, directly measured with the filter and a photomultiplier, is similar to the evolution of the total emission. The major part of the light is emitted during the breakdown and approximately during the first 500 ns [22]. We can thus conclude that the H_α line is emitted by the whole plasma volume. This can be understood considering the fact that the plasma is formed by cracking and ionizing the dielectric molecules and atoms. Since the hydrogen source is the dielectric, hydrogen atoms are present everywhere in the plasma. However, this is not the case for atoms coming from the electrodes (see § 3.3.).

The evolution of the plasma size is a more delicate point. Care has to be taken for the image treatment and interpretation. First, the light emitting region (excited region) could be broader than the plasma itself (ionized region). Secondly, the images have to be normalized in intensity. If not, the plasma seems to be bigger during the first microsecond, simply because the light intensity at this stage is much higher. Finally, we cannot acquire more than one image during a single discharge, because the CCD readout time is much longer than the discharge on-time. Thus, each image will be acquired during a different discharge. Since the discharges are poorly reproducible, the comparison between the images becomes difficult. However, figure 6 shows plasma images at different stages of the discharge. There is a slight growth of the emitting region, but its size remains fairly constant during the whole discharge.

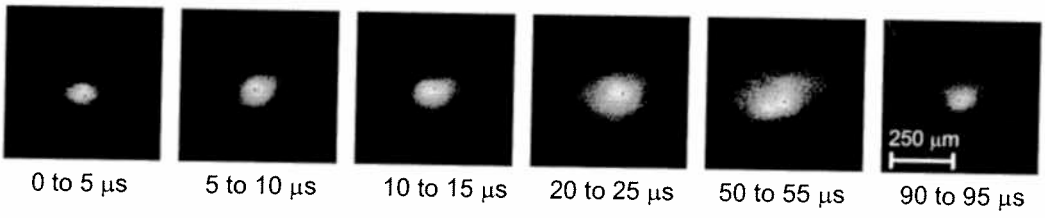

Figure 6. Plasma images at different times during the discharge (5 μs exposure, variable delay after breakdown; 24 A, 100 μs, water). The images are normalized in intensity. Each image is obtained during a different discharge.

Figure 7 shows fast imaging of the first 300 ns of the discharge. This time interval corresponds to the emission of the bright light peak observed in our previous paper [22]. It also corresponds to the first fast current rise, see figure 7. This interval is thus important in the plasma evolution: it is during the very beginning of the discharge that the plasma is developing and that a high amount of energy is brought into it.

The exposure time is 50 ns for each image, with variable delays. There is always a

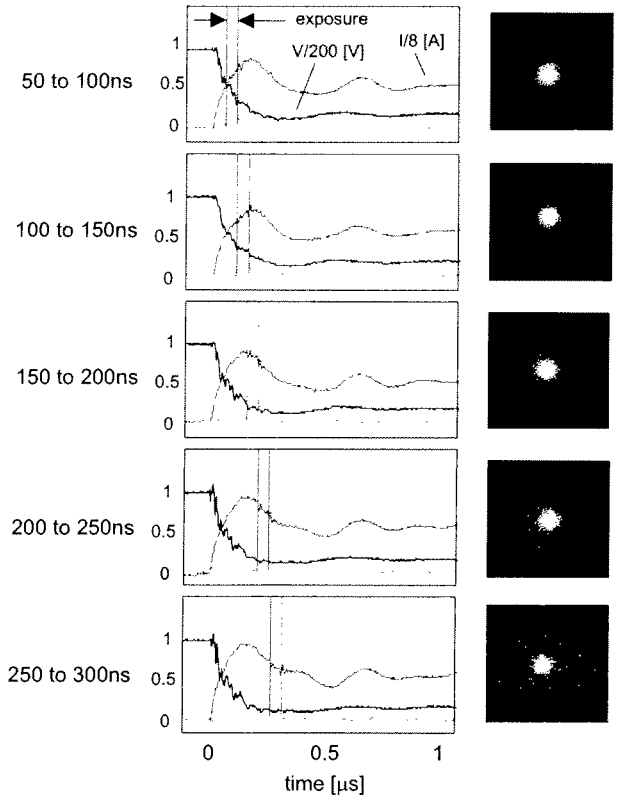

Figure 7. Fast imaging of the discharge beginning along with current and voltage evolution (50 ns exposure, variable delay; 6 A, water). The images are normalized in intensity. Each image is obtained during a different discharge.

50 ns intrinsic delay between the trigger signal (current rise at the breakdown) and the camera opening, due to gating electronics and cables. Since we cannot anticipate the breakdown for the camera triggering as previously mentioned, the first image can only be acquired 50 ns after the breakdown.

Between 100 and 200 ns after the breakdown, the current reaches its maximum. The light intensity is also at its maximum (images have a better signal to noise ratio). However, on the plasma images, no clear evolution is visible from 50 to 300 ns: size and geometry remain constant. Images obtained with delays longer than 300 ns are not shown here, but they are similar to those of the figure 7. This shows that the plasma is developing very fast (< 50 ns) after the breakdown, and then remains quite stable.

We have also investigated the afterglow of the discharge. The current and the voltage are shut down and drop rapidly to zero. Simultaneously, the total light intensity, measured with a photomultiplier, is also dropping fast. But there is still a weak slowly-decaying light emission, typically until 400 μs after the end of the discharge. Figure 8(a) shows

an image acquired directly after a discharge, and figure 8(b) shows the optical spectrum of the post-discharge light.

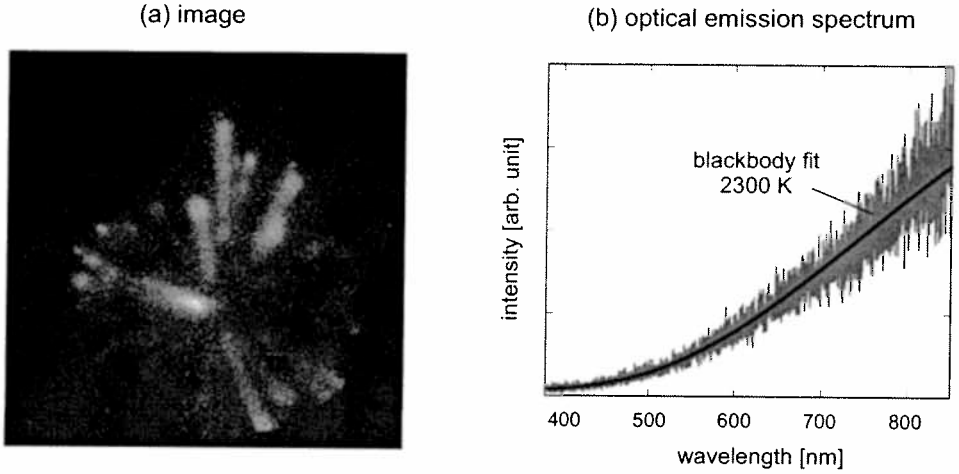

Figure 8. Incandescence of the removed particles after a discharge. (a) Image of a single post-discharge (100 μs exposure; 12 A, 50 μs, oil). (b) Optical emission spectrum, with a 2300 K blackbody fit. The light measurement is time integrated over thousands of post-discharges (50 μs exposure, 150 g/mm grating; 16 A, 50 μs, oil).

As shown in figure 8, the weak light emitted after the discharge is due to particles of heated metal. These particles are coming from the molten metal pool created in the workpiece during the discharge, and are then removed from the workpiece and ejected in the dielectric when the discharge is shut down. We see their path and not only luminous dots, because they are moving during the camera exposure. Spectroscopy shows that this post-discharge light emission is close to a blackbody radiation, which confirms that the emitters are heated metal particles. The spectrum in figure 8(b) is quite noisy, due to the low intensity of the afterglow emission. Fitting the afterglow spectra with Planck's law, the temperature of the emitters is found to be around 2200 K ($\pm$ 100 K). Since the melting point of steel is $\sim$ 1700 K, the particles are still in a liquid state in the very beginning of the post-discharge.
The particle size can be measured on the images. We found that the largest particles have a diameter of $\sim$ 30 μm, which is consistent with previous work on spark-eroded particles [33, 34]. The particle speed can also be estimated from images. The maximum speed is around 3 m/s.

3.3. Spatially-resolved optical emission spectroscopy

In order to have sufficient light intensity for spectroscopy, the light from thousands of discharges is accumulated over several seconds. Figure 9 shows spatially-resolved spectra (along a vertical axis) of an interesting spectral region for plasma contamination measurements. Near 520 nm are located three intense lines of neutral chromium (at

520.45, 520.6 and 520.84 nm) and one intense line of neutral copper (at 521.82 nm). Since we use a copper electrode and a stainless steel workpiece, the Cu line is emitted by particles coming from the electrode and the Cr lines are emitted by particles coming from the workpiece.

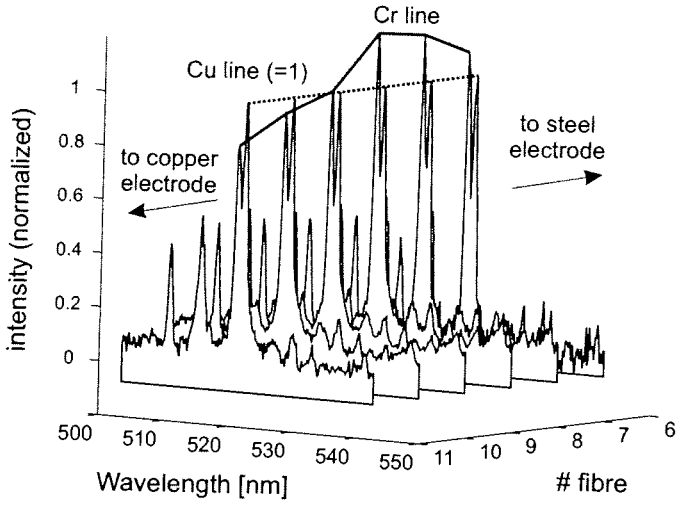

Figure 9. Vertical asymmetry of the plasma contamination observed with spatially-resolved spectroscopy. The spectra are normalized to the intensity of the Cu line at 521.8 nm. The light measurement is time integrated over thousands of discharges (6 A, 100 μs, water, 150 g/mm grating)

An asymmetry of the plasma contamination is clearly visible. Near the Cu electrode, the Cu line is more intense than the Cr lines. On the other hand, the Cr lines are more intense than the Cu line near the steel workpiece. Thus, we see that each electrode is contaminating the plasma mostly in a region close to itself.

Depending on the discharge parameters, material transfer from one electrode to the other can sometimes be observed. In this case, the intensity of lines emitted by both electrode materials are quite constant across the profile. With the discharge conditions of figure 9, no material transfer is macroscopically visible on the electrodes after several minutes of machining. This is qualitatively confirmed by the contamination asymmetry measured by spatially-resolved spectroscopy.

The electron density was calculated from H_α line broadening measurements [35]. In dense plasmas such as EDM plasma, line broadening is by far dominated by Stark broadening [36]. From H_α full width at half maximum measurements, the electron density has been determined using calculations of Gigosos and Cardenoso on hydrogen Stark broadening [37]. Figure 10 shows spatially-resolved H_α spectra, along with the electron density vertical profile calculated from them. The central spectra have a better signal to noise ratio than the outer ones, because the light intensity is higher in the center (see § 3.2.).

The values found are in good agreement with our previous results, around 5×10^{16} cm^{-3}

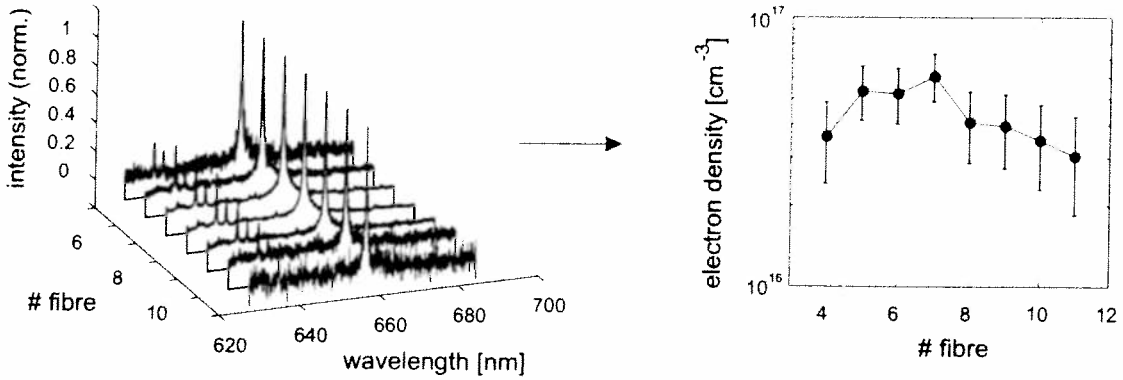

Figure 10. Vertical profile of the electron density calculated from spatially-resolved H_α broadening measurements. The spectra are normalized to the intensity of the H_α line at 656.2 nm. The light measurement is time integrated over thousands of discharges (6 A, 100 μs, water, 600 g/mm grating)

for a 100 μs discharge [22]. Despite large error bars, the electron density seems to be slightly higher in the plasma centre.

Calculations of the electron temperature can be done with the Boltzmann plot method, based on line intensity ratio measurements [35]. Here we have used three lines emitted by neutral copper, at 510.55, 515.32 and 521.82 nm. Since these lines are located in the same spectral region, we can assume that the overall spectral transmission is the same for the three lines. It should be noted that the Boltzmann plot method requires the assumption of a plasma in local thermal equilibrium (LTE). It is not an obvious assumption, especially for non-ideal plasmas like EDM plasmas [22]. Thermal interactions are comparable to coulombian interactions in such plasmas. The evolution to the equilibrium state by thermal interactions is thus perturbed by coulombian effects. However, due to the high plasma density, one can assume that the numerous collisions between particles thermalize them rapidly. The assumption of LTE can thus reasonably be accepted.

Spatially-resolved spectra of the three Cu lines are shown in figure 11, along with the electron temperature vertical profile. The electron temperature is quite constant over the whole profile. The plasma has thus a homogeneous electron temperature around 0.7 eV (8100 K), as previously measured [22].

4. CONCLUSIONS

The experimental investigation of the EDM plasma is complex, mostly because of its small size and its poor reproducibility. As shown here, the breakdown has a stochastic nature. This is another experimental difficulty, especially for triggering the diagnostics. During the pre-breakdown, fast current peaks (associated with streamer propagation) and gas bubbles are observed in water but not in oil. The presence of bubbles created

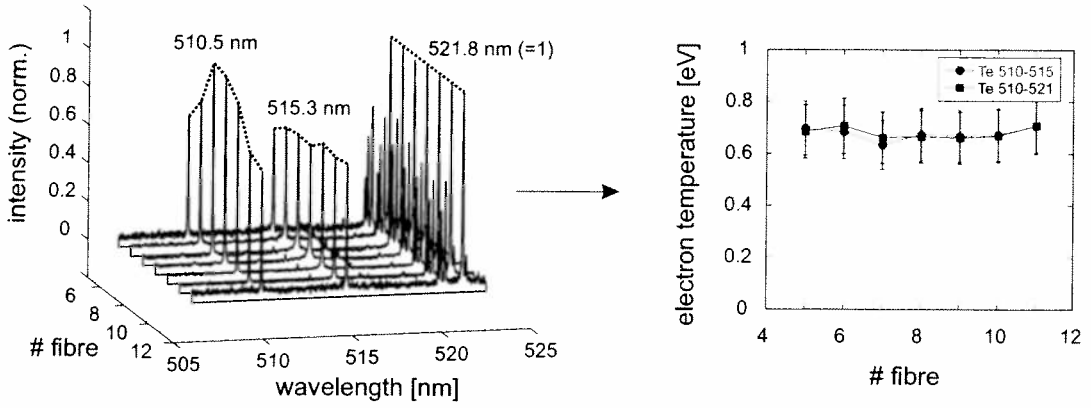

Figure 11. Vertical profile of the electron temperature calculated from spatially-resolved Cu lines intensities ratios. The spectra are normalized to the intensity of the Cu line at 521.8 nm. The light measurement is time integrated over thousands of discharges (6 A, 100 μs, water, 1800 g/mm grating)

by electrolysis of water could lead to a different breakdown mechanism from the one in oil. Imaging shows that the plasma develops very fast (< 50 ns) and then remains quite stable during the rest of the discharge. The plasma excites a broad volume around the gap ($\sim$ 50-400 μm in diameter, depending on the discharge current), but the light emission is much stronger in the central region, i.e. in the gap between the electrodes. Since hydrogen is coming from the dielectric, the H_α line is emitted by the whole plasma. On the contrary, the plasma contamination coming from the electrodes is located mostly close to them, as we can see with spatially-resolved spectroscopy. Images taken directly after a discharge show the incandescent particles removed from the workpiece. Using Planck's law, their temperature is around 2100 K in the very beginning of the post-discharge, which indicates that they are still in a liquid state. The vertical profile of the electron density has been measured with spatially-resolved spectra of the H_α line. The density is calculated from Stark broadening measurements. The electron density seems to be a little higher in the center of the plasma, around 5×10^{16} cm^{-3} for the chosen discharge parameters. Similarly, the vertical profile of the electron temperature is calculated with the Boltzmann plot method, from spatially-resolved spectra of three Cu lines. The electron temperature is quite constant around 0.7 eV. These profile measurements can be useful for EDM plasma modelling.

Acknowledgments

This work is funded by the Swiss Federal Research grant TopNano 21, project n° 5768.2.

References

[1] Lazarenko B R 1943 *About the inversion of metal erosion and methods to fight ravage of electric contacts* WEI-Institut, Moscow (in Russian)
[2] Germer L H and Haworth F E 1949 *J. Appl. Phys.* **20** 1085
[3] Cobine J D and Burger E E 1955 *J. Appl. Phys.* **26** 895
[4] Zingerman A S 1956 *Sov. Phys. Tech. Phys* **1** 1945
[5] Ho K H and Newman S T 2003 *Int. J. Mach. Tools and Manufacture* **43** 1287
[6] Ho K H, Newman S T, Rahimifard S and Allen R D 2004 *Int. J. Mach. Tools and Manufacture* **44** 1247
[7] Lauwers B, Kruth J P, Liu W, Eeraerts W, Schacht B and Bleys P 2004 *J. Mater. Process. Technol.* **149** 347
[8] Tani T, Fukuzawa Y, Mohri N, Saito N and Okada M 2004 *J. Mater. Process. Technol.* **149** 124
[9] Takezawa H, Hamamatsu H, Mohri N and Saito N 2004 *J. Mater. Process. Technol.* **149** 112
[10] Fleischer J, Masuzawa T, Schmidt J and Knoll M 2004 *J. Mater. Process. Technol.* **149** 246
[11] Beltrami I, Joseph C, Clavel R, Bacher J-P and Bottinelli S 2004 *J. Mater. Process. Technol.* **149** 263
[12] Cusanelli G, Hessler-Wyser A, Bobard F, Demellayer R, Perez R and Flükiger R 2004 *J. Mater. Process. Technol.* **149** 289
[13] Klocke F, Lung D, Antonoglu G and Thomaidis D 2004 *J. Mater. Process. Technol.* **149** 191
[14] Das S, Klotz M and Klocke F 2003 *J. Mater. Process. Technol.* **142** 434
[15] Perez R, Rojas H, Wälder G and Flükiger R 2004 *J. Mater. Process. Technol.* **149** 198
[16] Schulze H-P, Herms R, Juhr H, Schätzing W and Wollenberg G 2004 *J. Mater. Process. Technol.* **149** 316
[17] Van Dijck F 1973 *Physico-mathematical analysis of the electro discharge machining process* (Ph.D. dissertation, Catholic University of Leuven, Belgium)
[18] DiBitonto D D, Eubank P T, Patel M R and Barrufet M A 1989 *J. Appl. Phys.* **66** 4095
[19] Patel M R, Barrufet M A, Eubank P T and DiBitonto D D 1989 *J. Appl. Phys.* **66** 4104
[20] Eubank P T, Patel M R, Barrufet M A and Bozkurt B 1993 *J. Appl. Phys.* **73** 7900
[21] Albinski K, Musiol K, Miernikiewicz A, Labuz S and Malota M 1996 *Plasma Sources Sci. Technol.* **5** 736
[22] Descoeudres A, Hollenstein Ch, Demellayer R and Wälder G 2004 *J. Phys. D: Appl. Phys.* **37** 875
[23] Schumacher B M 2004 *J. Mater. Process. Technol.* **149** 376
[24] Rehbein W, Schulze H-P, Mecke K, Wollenberg G and Storr M 2004 *J. Mater. Process. Technol.* **149** 58
[25] Chadband W G 1992 (March) *Power Engineering Journal* 61
[26] Devins J, Rzad S and Schwabe R 1981 *J. Appl. Phys.* **52** 4531
[27] Lesaint O and Gournay P 1994 *IEEE Trans. on Diel. and Electr. Insul.* **1** 702
[28] Beroual A, Zahn M, Badent A, Kist K, Schwabe A J, Yamashita H, Yamazawa K, Danikas M, Chadband W G and Torshin Y 1998 *IEEE Electr. Insul. Mag.* **14** 6
[29] Frayssines P, Bonifaci N, Denat A and Lesaint O 2002 *J. Phys. D: Appl. Phys.* **35** 369
[30] Weibull W 1951 *J. Appl. Mech.* **18** 293
[31] Frei C J 1985 *IEEE Trans. on Electr. Insul.* **20** 303
[32] Frei C J, He L and Müller K 1989 *IEEE Trans. on Electr. Insul.* **24** 169
[33] Berkowitz A E and Walter J L 1987 *J. Mater. Res.* **2** 277
[34] Carrey J, Radousky H B and Berkowitz A E 2004 *J. Appl. Phys.* **95** 823
[35] Griem H R 1997 *Principles of Plasma Spectroscopy* (Cambridge: University Press)
[36] Griem H R 1974 *Spectral Line Broadening by Plasmas* (New York: Academic Press)
[37] Gigosos M A and Cardenoso V 1996 *J. Phys. B: At. Mol. Opt. Phys.* **29** 4795